Chiral tunneling, tunneling times, and Hartman effect in bilayer graphene

Chang-Soo Park*
Department of Physics, Dankook University, Cheonan, 330-714, Republic of Korea
(Received 28 October 2013; revised manuscript received 10 February 2014; published 17 March 2014)

We investigate the chiral tunneling in a bilayer graphene n-p-n junction in time aspect. The phase and dwell times are evaluated for various situations, including the effects of trigonal warping and band gap due to an external gate field. In the absence of band gap and for normal incidence, the chirality induces Klein effects; when the trigonal warping is excluded, the tunneling times are the same as the ordinary barrier tunneling, but including it leads to a perfect reflection and a new type of phase time is found. In the presence of band gap and/or for an oblique incidence, the Klein effects disappear and the tunneling times have peaks corresponding to resonant transmission maxima due to the Fabry-Pèrot-type interference of the oscillating waves allowed inside the barrier. The trigonal warping also leads to valley-polarized transmission for an oblique incidence in the absence or presence of band gap. As a result, the tunneling times and scattering angles of particles from one valley are different from the other valley. We observe that the Hartman effect exists only when the chirality selects pure evanescent waves as transmission channels.

DOI: 10.1103/PhysRevB.89.115423 PACS number(s): 72.80.Vp, 03.65.Pm, 03.65.Xp

I. INTRODUCTION

Transport of quasiparticles in graphene [1–3] features many interesting phenomena, not familiar with electrons in conventional semiconductors. In particular, their chiral properties control the flow of quasiparticles in graphene junctions, rendering the Klein effects [4,5]; for normal incidence on a potential barrier, the quasiparticles of monolayer graphene (MLG) are perfectly transmitted through the barrier and those of bilayer graphene (BLG) have exponentially small transmission probability even if there are many empty states inside the barrier [6–9]. There have been many studies on the perfect transmission in MLG [6,10,11] and experimental results have also been reported [12–14]. In recent years, the chirality-induced Klein effects in BLG have drawn more attention [15–20] because of its potential device applications due to the tunability of band gap [21–27].

In this paper, we study the chiral tunneling of quasiparticles in a BLG n-p-n junction, including the effects of trigonal warping (TW) and band gap induced by an external electric field applied perpendicularly to the layer. In particular, we investigate the chiral tunneling in connection with tunneling times, namely, the phase and dwell times. Previously, the effect of band gap on the chiral tunneling has been discussed in view of Zener tunneling [15], survival of the Klein effect [17] and the effects of magnetic barrier [18]. In these and other studies [6,9] the TW term has been discarded by assuming the low-energy dispersion is dominated by the quadratic term. As we show below, however, the inclusion of the TW makes the transmission of quasiparticles through a barrier qualitatively different from the case without it, in the absence or presence of band gap, and the difference between the two cases can be seen clearly in the behaviors of the tunneling times. The essential features of transmission through the BLG junction are determined by the chirality of pseudospinors which are strongly coupled to the nature of wave vectors. When the TW is included complex wave vectors as well as real or imaginary wave vectors appear, which makes the transmission diverse. By carefully examining these wave vectors in association with the chirality, we analyze the effects of the TW and band gap on the transmission. For the normal incidence, a perfect reflection of particles is observed when the TW is included in the absence of band gap. For an oblique incidence, in the absence or presence of band gap, the TW leads to valley-dependent transmission times because of the break of the valley symmetry. We also examine the existence of the Hartman effect in the BLG junction by simulating dependence of the tunneling times on barrier width. We find that the Hartman effect can exist for the quasiparticles of normal incidence when there is no band gap and the TW term is excluded.

The paper is organized as follows. In Sec. II, we present the general low-energy eigenspectrum and eigenfunction of quasiparticles when both the TW term and band gap are included. We then describe the barrier tunneling in the Klein-effect regime and define a chirality-dependent transition probability between incident and scattered pseudospinors. In Sec. III, we use the transition probability to analyze the chiral tunnelings for four different situations (with and without the TW term, both in the absence and presence of band gap), and evaluate the tunneling times as functions of incident energy and barrier width for each situation. Finally, conclusion with remarks will be present in Sec. IV.

II. BARRIER TUNNELING IN BLG

A. Low-energy eigenspectrum and eigenfunction

The low-energy effective Hamiltonian of BLG in the presence of band gap, including the TW term, is given by [28–31]

$$\hat{\mathcal{H}} = \begin{pmatrix} \tau u\left(1 - \frac{v_F^2}{\gamma_1^2}\hat{\pi}^\dagger\hat{\pi}\right) & -\frac{1}{2m}(\hat{\pi}^\dagger)^2 + \tau v_3\hat{\pi} \\ -\frac{1}{2m}\hat{\pi}^2 + \tau v_3\hat{\pi}^\dagger & -\tau u\left(1 - \frac{v_F^2}{\gamma_1^2}\hat{\pi}\hat{\pi}^\dagger\right) \end{pmatrix}, \quad (1)$$

where $\hat{\pi} = \hat{p}_x + i\hat{p}_y$ ($\hat{p}_{x,y} = -i\hbar\partial_{x,y}$), $m = \gamma_1/2v_F^2$ is an effective mass, with the Fermi velocity v_F [32] and $\gamma_1 \approx 0.4$ eV, and τ is the valley index, with $\tau = +1$ for the K

*olnal@dankook.ac.kr

valley and $\tau = -1$ for the K' valley. The effective velocity $v_3 = \gamma_3 v_F/\gamma_0 = 0.107 v_F$ ($\gamma_3 \approx 0.3$ eV, $\gamma_0 \approx 2.8$ eV) causes the TW distortion to the energy dispersion and u is the band-gap parameter due to an external gate field. At very low energy, the TW term leads to the Lifshitz transition, splitting the eigenspectrum into four Dirac cones each with linear dispersion [28,29]. The theoretical value of the transition energy is $E_L = \gamma_1(\gamma_3/2\gamma_0)^2 \sim 1$ meV but the experimentally observed value is $E_L \sim 6$ meV [33]. The effect of the TW on the electronic spectrum and transport near E_L has been discussed in Ref. [34]. In this paper, we assume $E > E_L$.

The low-energy eigenspectrum of quasiparticles, satisfying the eigenvalue equation $\hat{\mathcal{H}}|\psi_{\tau s}(\boldsymbol{k})\rangle = E_{\tau s}(\boldsymbol{k})|\psi_s(\boldsymbol{k})\rangle$, is

$$E_{\tau s}(\boldsymbol{k}) = s E_\tau(\boldsymbol{k}), \quad E_\tau(\boldsymbol{k}) = \sqrt{\lambda_{\tau k}^2 + \lambda_u^2},$$
$$\lambda_{\tau k} = \sqrt{\epsilon_k^2 + \epsilon_{3k}^2 - 2\tau\epsilon_k\epsilon_{3k}\cos 3\theta}, \quad \lambda_u = u - \epsilon_u, \tag{2}$$
$$\epsilon_k = \frac{\hbar^2 k^2}{2m}, \quad \epsilon_{3k} = \hbar k v_3, \quad \epsilon_u = \frac{\hbar^2 k^2}{2m_u}, \quad \theta = \arctan\frac{k_y}{k_x}.$$

Here, $m_u = \gamma_1^2/2uv_F^2$ is an effective mass associated with the band-gap parameter u, $\boldsymbol{k} = (k_x,k_y)$ with $k = \sqrt{k_x^2 + k_y^2}$ are two-dimensional (2D) wave vectors, and s is the band index with $s = +1$ and $s = -1$ for the conduction band and the valence band, respectively. In the plane-wave basis the eigenfunction, in its most general form, can be expressed as

$$\psi_{\tau s}(\boldsymbol{r}) = \frac{1}{\sqrt{2E_\tau}}\begin{pmatrix}\sqrt{E_\tau + \tau s\lambda_u}\\ -s\sqrt{E_\tau - \tau s\lambda_u}\, e^{i\delta_\tau}\end{pmatrix} e^{i\boldsymbol{k}\cdot\boldsymbol{r}}$$
$$\equiv |\chi_{\tau s}(\boldsymbol{k})\rangle\, e^{i\boldsymbol{k}\cdot\boldsymbol{r}}, \tag{3}$$
$$\delta_\tau(k,\theta) = \arctan\frac{\epsilon_k \sin 2\theta + \tau\epsilon_{3k}\sin\theta}{\epsilon_k\cos 2\theta - \tau\epsilon_{3k}\cos\theta},$$

where we have taken the sample size to be unity. In the above expression, the pseudospinor $|\chi_{\tau s}(\boldsymbol{k})\rangle$ represents the two sublattices and its explicit form varies depending on the situations that we shall discuss below. The simultaneous dependence on the band index s and wave vector $\boldsymbol{k}$ leads to the chiral property of the pseudospinor. To see this property, one can introduce a chirality operator, $\hat{C}_\tau(k) = \hat{\boldsymbol{\sigma}}\cdot\mathbf{n}_\tau(k)$ with $\mathbf{n}_\tau(k) = (-1/E_\tau)[\lambda_{\tau k}(\cos\delta_\tau\,\mathbf{e}_x + \sin\delta_\tau\,\mathbf{e}_y) - \tau\lambda_u\,\mathbf{e}_z]$, where $\hat{\boldsymbol{\sigma}}$ is the pseudospin vector represented by Pauli matrices [35] and $\mathbf{n}_\tau$ is the pseudospin polarization axis. The chirality operator then satisfies the eigenvalue equation $\hat{C}_\tau(k)|\chi_{\tau s}(k)\rangle = s|\chi_{\tau s}(k)\rangle$; the pseudospin vector $\boldsymbol{\sigma}$ is parallel or antiparallel to the polarization axis $\mathbf{n}_\tau$, depending on the band index s. As we shall see below, this chiral property plays an important role in the transmission of quasiparticles through a barrier.

B. Barrier interaction and Klein effect

We consider a BLG n-p-n junction in which the p region is described by a rectangular potential barrier with height V_0,

$$V(x,y) = \begin{cases} 0, & x < 0, x > d,\\ V_0, & 0 \leqslant x \leqslant d.\end{cases} \tag{4}$$

Here, we have assumed the potential barrier is translational invariant along the y direction, so that the y component of particle momentum is conserved. Using this, the wave equation for quasiparticles incident on the barrier can be conveniently written as

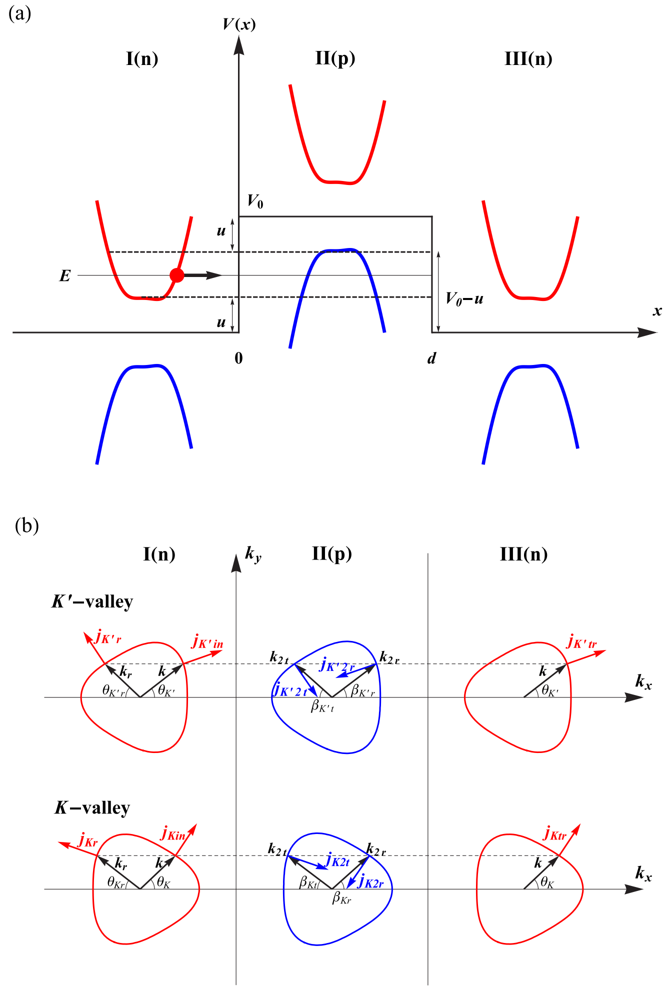

FIG. 1. (Color online) (a) Potential barrier and energy dispersions (including the TW) when $V_0 = 0.75\gamma_1$, $u = 0.25\gamma_1$ ($\gamma_1 = 0.4$ eV). The range $u < E < V_0 - u$ is the Klein-effect regime. (b) The isoenergy contours of the K and K' valleys when $E = 0.35\gamma_1$. $\boldsymbol{k}(\boldsymbol{k}_2)$ denote wave vectors and $\boldsymbol{j}$ are the particle fluxes whose directions are normal to the contour [see Eq. (10)]: note their directions are generally different from the corresponding wave vectors. The dashed lines indicate the conservation of k_y, that is, $k_y = k_{ry} = k_{2ty} = k_{2ry}$. θ (β_t) and θ_r (β_r) are the incident (transmission) and reflection (reflection) angles in zone I (II), respectively: note $\theta_r \neq \theta$ because $|\boldsymbol{k}| \neq |\boldsymbol{k}_r|$ due to the anisotropy.

$$\hat{\mathcal{H}}\,\varphi_{\tau s}(x)e^{ik_y y} = \begin{cases} E\,\varphi_{\tau s}(x)e^{ik_y y}, & x < 0, \quad x > d,\\ -E_2\,\varphi_{\tau s}(x)e^{ik_y y}, & 0 \leqslant x \leqslant d,\end{cases} \tag{5}$$

where E is the Fermi energy and $E_2 = V_0 - E$, with $E < V_0$. We are interested in the tunneling in the Klein-effect regime where the conduction bands outside the barrier overlap the valence band inside the barrier. In the presence of a band gap, the range of E and E_2 for the Klein effect is $u < E(E_2) < V_0 - u$ with $V_0 > 2u$ [see Fig. 1(a)] [36].

The energy $E_{\tau s}(\boldsymbol{k})$ in Eq. (2) is a quartic function of the wave vector k and hence, for a given energy $E = E_{\tau s}(\boldsymbol{k})$, four roots of k are possible in the complex regime. Taking into account this and assuming the particles are incident from the left n region we write the wave functions at each region, apart from the translational-invariant part $e^{ik_y y}$, as follows:

$$\begin{aligned} \varphi_{\mathrm{I}}(x) &= \begin{pmatrix} i_1 \\ i_2 e^{i\delta_\tau} \end{pmatrix} e^{ik_{ix}x} + R_\tau \begin{pmatrix} r_1 \\ r_2 e^{i\delta_{\tau r}} \end{pmatrix} e^{-ik_{rx}x} \\ &\quad + A_\tau \begin{pmatrix} a_1 \\ a_2 e^{i\eta_{1\tau}} \end{pmatrix} e^{iq_{1x}x}, \\ \varphi_{\mathrm{II}}(x) &= B_\tau \begin{pmatrix} b_1 \\ b_2 e^{i\delta_{2\tau r}} \end{pmatrix} e^{ik_{2rx}x} + C_\tau \begin{pmatrix} c_1 \\ c_2 e^{i\delta_{2\tau t}} \end{pmatrix} e^{-ik_{2tx}x} \\ &\quad + D_\tau \begin{pmatrix} d_1 \\ d_2 e^{i\eta_{2\tau+}} \end{pmatrix} e^{iq_{2x+}x} + F_\tau \begin{pmatrix} f_1 \\ f_2 e^{i\eta_{2\tau-}} \end{pmatrix} e^{iq_{2x-}x}, \\ \varphi_{\mathrm{III}}(x) &= T_\tau \begin{pmatrix} t_1 \\ t_2 e^{i\delta_\tau} \end{pmatrix} e^{ik_x x} + G_\tau \begin{pmatrix} g_1 \\ g_2 e^{i\eta_{3\tau}} \end{pmatrix} e^{iq_{3x}x}, \end{aligned} \tag{6}$$

where all k values are positive real and q can have pure imaginary or complex values. As depicted in Eq. (3), the pseudospinors depend on the band index as well as the wave vectors due to the chirality. The phase factors for real wave vectors are, with the expression of $\delta_\tau(k,\theta)$ given in Eq. (3),

$$\begin{aligned} \delta_{\tau r} &= \delta_\tau(k_r, \pi - \theta_r), \\ \delta_{2\tau r} &= \delta_\tau(k_{2r}, \beta_r), \\ \delta_{2\tau t} &= \delta_\tau(k_{2t}, \pi - \beta_t), \end{aligned} \tag{7}$$

where θ_r, β_t, and β_r are positive angles, as defined in Fig. 1(b); note the reflection (transmission) angle at region I (II) is thus $\pi - \theta_r$ ($\pi - \beta_t$). These angles are determined by the following conservation relation for the y-component of momentum due to the translational invariance:

$$k \sin\theta = k_r \sin\theta_r = k_{2t} \sin\beta_t = k_{2r} \sin\beta_r. \tag{8}$$

The phase factors η_τ for the imaginary or complex wave vectors can also be obtained from $\delta_\tau(k,\theta)$; $\eta_\tau = \delta_\tau(q,\theta_c)$, where θ_c are complex (or imaginary) arguments determined from the following relation,

$$k \sin\theta = q_1 \sin\theta_{1c} = q_2 \sin\theta_{2c}. \tag{9}$$

As illustrated in Fig. 1(b), the usual law of reflection does not hold here because the anisotropic dispersion due to the TW leads to $|\boldsymbol{k}| \neq |\boldsymbol{k}_r|$. Moreover, the particle flux is, in general, not parallel (or antiparallel) to the direction of the wave vectors $\boldsymbol{k}$. To see this we note that the particle flux, in the presence of the TW and band gap, is defined as follows:

$$\begin{aligned} \boldsymbol{j}_{\tau s} &= \langle \psi_{\tau s} | \hat{\boldsymbol{v}} | \psi_{\tau s} \rangle \quad \leftarrow \quad \hat{\boldsymbol{v}} = \frac{1}{i\hbar}[i\hbar \nabla_{\boldsymbol{p}}, \hat{\mathcal{H}}(\boldsymbol{p})] \\ &= \frac{s}{E_\tau}[\lambda_{\tau k}(v_k \cos(\delta_\tau - \theta) - \tau v_3 \cos\delta_\tau) - \lambda_u v_u \cos\theta]\mathbf{e}_x \\ &\quad + \frac{s}{E_\tau}[\lambda_{\tau k}(v_k \sin(\delta_\tau - \theta) - \tau v_3 \sin\delta_\tau) - \lambda_u v_u \sin\theta]\mathbf{e}_y, \end{aligned} \tag{10}$$

where $v_k = \hbar k/m$, $v_u = \hbar k/m_u$, and $\nabla_{\boldsymbol{p}} = \partial_{p_x}\mathbf{e}_x + \partial_{p_y}\mathbf{e}_y$ [see also (A1)]: note $\boldsymbol{j}_{\tau s}$ is the same as the group velocity $\boldsymbol{v}_{\tau s} = s(1/\hbar)\nabla_{\boldsymbol{k}} E_\tau(\boldsymbol{k})$ under proper normalization. Clearly, the direction of $\boldsymbol{j}_{\tau s}$ is different from the wave vectors, except when $\theta = 0$. We also remark that the anisotropy leads to a valley-dependent range of the incident angle θ, which is determined by the positiveness of the x component of the flux; the range of $|\theta|$ can be larger than $\pi/2$ for the K valley and less than $\pi/2$ for the K' valley.

Viewing the interaction of quasiparticles with the potential barrier as a scattering the transition probability from the incident wave $e^{i\boldsymbol{k}_i\cdot\boldsymbol{r}}$ to a scattered wave, within the first Born approximation and assuming no intervalley scattering is allowed, can be described by $\mathcal{P}_{fi} = |\langle \psi_{\tau s_f}(\boldsymbol{k}_f)|V(\boldsymbol{r})|\psi_{\tau s_i}(\boldsymbol{k}_i)\rangle|^2 \propto W(\boldsymbol{k}_f,\boldsymbol{k}_i)$ [7,37]. Here, $\boldsymbol{k}_i$ and $\boldsymbol{k}_f$ are the incident and scattered wave vectors, respectively, and $W(\boldsymbol{k}_f,\boldsymbol{k}_i)$ is a chirality-dependent scattering probability between the incident pseudospinor and a scattered pseudospinor, given by

$$\begin{aligned} &W(\boldsymbol{k}_f,\boldsymbol{k}_i) \\ &\quad = \left|\left\langle \chi_{\tau s_f}(\boldsymbol{k}_f) \middle| \chi_{\tau s_i}(\boldsymbol{k}_i)\right\rangle\right|^2 \\ &\quad = \frac{E_{\tau i}E_{\tau f} + s_i s_f\left[\lambda_{u_i}\lambda_{u_f} + \lambda_{\tau k_i}\lambda_{\tau k_f}\cos(\delta_{\tau f} - \delta_{\tau i})\right]}{2E_{\tau i}E_{\tau f}}, \end{aligned} \tag{11}$$

where $\delta_{\tau i} = \delta_\tau$ and we have used the expression (3) in the second line. The band indices s_i and s_f have the properties of $s_i s_f = -1$ for the transmission across a junction and $s_i s_f = +1$ for the reflection within a junction. As we shall see shortly, this chirality-dependent transition probability allows or forbids scattering from the incident wave to a state corresponding to a particular wave vector inside or outside the barrier region, so that a selective transmission arises, known as the Klein effect.

III. TUNNELING TIMES IN THE KLEIN-EFFECT REGIME

Having obtained the eigenspectrum and described the barrier interaction of quasiparticles, we now discuss tunneling (or interaction) times in the BLG junction. Among many controversial definitions the following two are generally accepted as well established concepts of tunneling times, namely, the phase time t_{ph} and the dwell time t_D [38,39]:

$$t_{\mathrm{ph}} = \hbar\frac{\partial\Delta\phi}{\partial E}, \quad t_D = \frac{1}{|\boldsymbol{j}_{\mathrm{in}}|}\int_0^d \varphi^\dagger(x)\varphi(x)\,dx. \tag{12}$$

In the above expressions, $\Delta\phi$ is the phase delay due to the barrier and $\boldsymbol{j}_{\mathrm{in}}$ is the incident flux of particles normal to the barrier, that is, the x-component of $\boldsymbol{j}_{\tau s}$ defined in Eq. (10). For ordinary barrier tunneling the two tunneling times exhibit a peculiar phenomenon, called the Hartman effect; the phase and dwell times become independent of the barrier thickness in the limit of opaque barrier [40]. In the following, we will investigate these tunneling times for the four different situations in the BLG junction.

A. Tunneling times when the TW is excluded

In this case, since $v_3 = 0$, the eigenspectrum has isotropic dispersion; the wave vectors have no valley dependence and the particle flux $\boldsymbol{j}_{\tau s}$ is parallel (antiparallel) to wave vector $\boldsymbol{k}$ in the conduction (valence) band. From Eq. (2), $E_\tau = \sqrt{\epsilon_k^2 + \lambda_u^2}$, and for a given energy $E = E_\tau$ the wave vectors have two real or two imaginary values, each with opposite signs; see Appendix B 1 for explicit expressions of the wave vectors. Thus the wave functions are pure oscillating or evanescent waves. In the following, we will first consider the case without band gap, then discuss the effect of the band gap.

1. In the absence of band gap

In this case, since $u = 0$ and $v_3 = 0$, we have $\delta_\tau = 2\theta$ and the x component of the pseudospinor eigenfunction in Eq. (3) can be written as

$$\varphi_{\tau s}(x) = \frac{1}{\sqrt{2}}\begin{pmatrix} 1 \\ -se^{\pm 2i\theta}\end{pmatrix} e^{\pm i k_x x} \quad \text{or} \quad \frac{1}{\sqrt{2}}\begin{pmatrix} 1 \\ se^{\pm 2\theta_\kappa}\end{pmatrix} e^{\pm \kappa_x x}, \tag{13}$$

where $k = \kappa = (1/\hbar)\sqrt{2mE}$ with the relation $E = [-\epsilon_k]_{k\to -i\kappa}$ [see Eq. (B2) for the regional wave vectors] and θ_κ is a positive value, satisfying the relation $\sinh\theta_\kappa = -\sin\theta$ from Eq. (9) [41]. The transition probability (11) for these pseudospinors is

$$W(k_f,k_i) = \tfrac{1}{2}[1 + s_i s_f \cos 2(\theta_f - \theta_i)], \tag{14}$$

where $\theta_i = \theta$ is the incident angle and θ_f is a scattering angle; $\theta_f = \pi - \beta_t$ or $\pm\theta_{\kappa_2}$ for the transmission and $\pi - \theta_r$ or θ_κ for the reflection. Note that $\cos 2(\theta_f - \theta) \to e^{\pm 2\theta_\kappa}\cos 2\theta$ for the imaginary wave vectors $-i\kappa$. From this relation, since $s_i s_f = -1$ for the transmission across a junction, we can see $W = 0$ when $\theta_f = \theta_i$ or $\theta_f = \theta_i + \pi$. According to the choice of angle convention described in Fig. 1(b), for the present case of isotropic dispersion, the range of scattering angle is $\pi/2 < \theta_f \leqslant \pi$, whereas the incident angle is in the range $0 \leqslant \theta_i < \pi/2$: the former condition never happens and the latter can be satisfied only when $\theta_i = 0$, that is, the normal incidence. Thus $W(k_{2t},k) = 0$ when $\theta = 0$, which implies that the transition to oscillating waves inside the barrier region are forbidden for the normal incidence. For an oblique incidence, however, we always have $W \neq 0$ and hence transitions to oscillating waves, as well as evanescent waves, inside the barrier are allowed.

Based on the above general analysis, we now discuss about the tunneling times. First, for the normal incidence, since $\theta_i = 0$, we find $W(\pm\kappa_2,k) = 1$ for the transmission and, for the reflection within a junction, since $s_i s_f = +1$, we obtain $W(-k_r,k) = 1$, $W(\kappa,k) = 0$. Thus the incident wave is transmitted through the barrier via only the evanescent waves $e^{\pm\kappa_2 x}$ because scattering into the oscillating waves are forbidden. This selective transmission is the Klein effect in the BLG barrier junction [6]. Since the transmission channels are the evanescent waves the situation is the same as the ordinary barrier tunneling from Schrödinger equation. In fact, from the matching conditions at boundaries, one can find exactly the same results for the transmission and reflection amplitudes, T and R, as in the ordinary barrier tunneling:

$$\begin{aligned} T &= |T|e^{-ikd}e^{i\Delta\phi}, \quad R = |R|e^{-i\pi/2}e^{-ikd}e^{i\Delta\phi}, \\ |T| &= \frac{2k\kappa_2}{\sqrt{4k^2\kappa_2^2 + \left(k^2+\kappa_2^2\right)^2\sinh^2(\kappa_2 d)}}, \\ \Delta\phi &= \arctan\left(\frac{k^2-\kappa_2^2}{2k\kappa_2}\tanh(\kappa_2 d)\right), \end{aligned} \tag{15}$$

where $|R|^2 = 1 - |T|^2$, $\Delta\phi$ is the phase delay due to the barrier, and the valley index τ and subscript x have been omitted because of the isotropic dispersion and $k_x = k$ for the normal incidence.

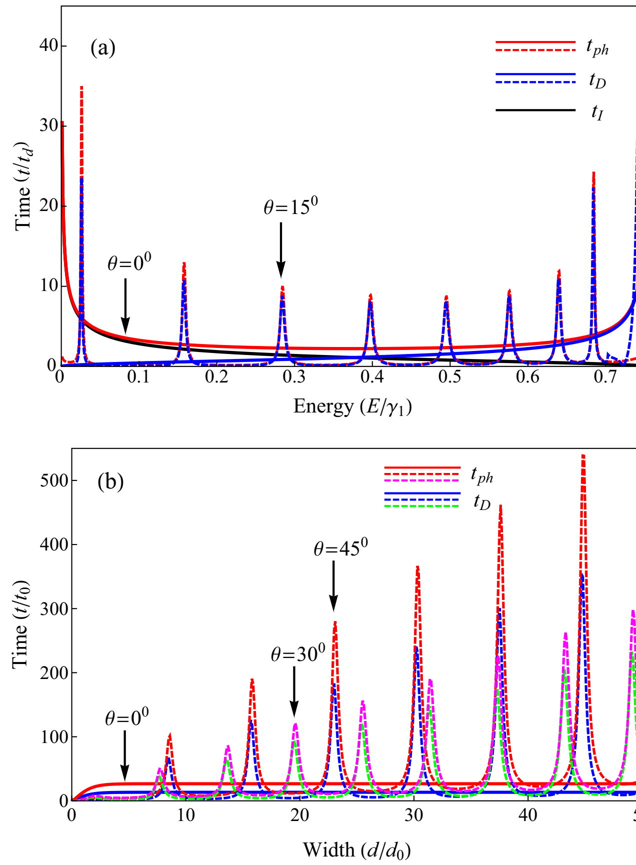

FIG. 2. (Color online) Tunneling times when ($u = 0$, $v_3 = 0$). (a) Phase ($t_{\rm ph}$), dwell (t_D), and interference (t_I) times vs energy for a barrier of width $d = 30d_0$: the solid lines are normal incidence ($\theta = 0°$), with magnitudes being 25 times scaled up for comparison. (b) The phase and dwell times as a function of barrier width when $E = 0.375\gamma_1$. The solid lines are normal incidence ($\theta = 0°$), with magnitudes being 10 times scaled up. Note they approach constant values as $d \to \infty$, exhibiting the Hartman effect. In both cases, $V_0 = 0.75\gamma_1$ ($\gamma_1 = 0.4$ eV), $d_0 = \hbar v_F/\gamma_1 = 1.48$ nm and the time units are $t_0 = d_0/v_F = 1.65$ fs and $t_d = d/v_F = 50t_0 = 82.5$ fs.

The phase and dwell times for the above results are well known and we reproduce them in Fig. 2(a) (see the solid lines indicated by $\theta = 0°$) [42]. We have also plotted the interference time t_I (solid black line) due to the self-interference delay in front of the barrier. According to Winful [43], a relationship $t_{\rm ph} = t_D + t_I$ is held for a barrier tunneling. To see if this relationship holds for the BLG junction, we follow Smith [44] to derive

$$\begin{aligned} \int_0^d \psi^\dagger\psi\, dx &= \left[\psi^\dagger \hat{M}\frac{\partial^2\psi}{\partial x\partial E} - \frac{\partial\psi^\dagger}{\partial x}\hat{M}\frac{\partial\psi}{\partial E} - i\hbar v_3\psi^\dagger\hat{\sigma}_x\frac{\partial\psi}{\partial E}\right]_0^d, \\ \hat{M} &= \frac{\hbar^2}{2m}\hat{\sigma}_x + \frac{\hbar^2}{2m_u}\hat{\sigma}_z, \end{aligned} \tag{16}$$

where $\hat{\sigma}$ are the Pauli matrices. Using this relation, with $v_3 = 0$ and $u = 0$, we verify the same relationship $t_{\rm ph} = t_D + t_I$ can hold in the BLG junction, where t_I, the self-interference delay time, is given as $t_I = (\hbar\partial \ln k/\partial E)|R| \cos\Delta\phi$. This is in contrast to the results for monolayer graphene in which the phase time is equal to the dwell time [45]. The main reason for this difference lies in their dispersion relations: linear dispersion in the MLG while quadratic dispersion in the BLG.

In Fig. 2(b), we also display the tunneling times as a function of the barrier width (see the solid lines indicated by $\theta = 0^\circ$). As can be expected from the analogy with the ordinary barrier tunneling, the Hartman effect is clearly seen; $t_{\rm ph}$ and t_D become constant in the limit of large barrier width. It has been reported that there is no Hartman effect in monolayer graphene junction [46]. This is because the allowed wave vectors inside the barrier from scattering are real in MLG, so that the transmission channels are propagating waves instead of evanescent waves.

For an oblique incidence, since $W(k_f,k_i) \neq 0$ for all (real or imaginary) k_f, the transmission channels are hybrid of the oscillating and evanescent waves and hence these two kinds of waves will contribute to the transmission probability: the evanescent waves yield exponential decay, whereas the oscillating waves will undergo the Fabry-Pèrot-type interference between the forward ($e^{ik_{2rx}x}$) and backward ($e^{-ik_{2tx}x}$) propagating waves inside the barrier [see Fig. 1(b) for the directions of the wave vectors] to produce resonant transmission probabilities. From Fig. 2(a), we can see the effect of interference on the tunneling times (the dashed lines indicated by $\theta = 15^\circ$) arises as peaks corresponding to the resonant transmission probabilities [see also Fig. 3(a) for the matching between the peak positions and the resonant transmissions]: the interval between two adjacent peaks is $\Delta E_n = (2\pi\gamma_1 d_0/d\cos\beta_t)[\sqrt{V_0/\gamma_1} - (\pi d_0/d\cos\beta_t)(n+1/2)]$, with $d_0 = \hbar v_F/\gamma_1$ and n being positive integer satisfying $u < E_n < V_0 - u$, so that the peaks become closer as the incident energy approaches the barrier height.

In Fig. 2(b), as a consequence of the interference, we also observe periodically appearing peaks of tunneling times as the barrier width increases for the incidence angles $\theta = 30^\circ$ and 45°: the interval between two adjacent peaks is $\Delta d = \pi/(k_{2t}\cos\beta_t)$. More importantly, the tunneling times become longer as the barrier width increases, showing disappearance of the Hartman effect for an oblique incidence. In the ordinary barrier tunneling, where only evanescent waves exist inside the barrier, the Hartman effect has been explained by the saturation of number of particles under the barrier, accounting the phase and dwell times as storage times of probability density [43,47]. In the present case, however, we have also oscillating waves that propagate inside the barrier region; while the evanescent waves lead to exponentially small transmission probabilities, the oscillating waves propagate through the barrier without decay. In the limit of opaque barrier, the transmission of quasiparticles is thus dominated by the propagating waves, so that the particles can move with finite velocities inside the barrier. Apart from the amplitudes B and C in Eq. (6), the particle velocity can be obtained from (10), $v_{2tx} = v_{k_2}\cos(\beta_t - \theta)$, where $v_{k_2} = \hbar k_2/m$ and β_t is determined by the relation (8). Consequently, the quasiparticles will traverse the barrier at finite velocities to have increasing tunneling times as the barrier width increases and hence the Hartman effect disappears. In fact, as we shall see below, the Hartman

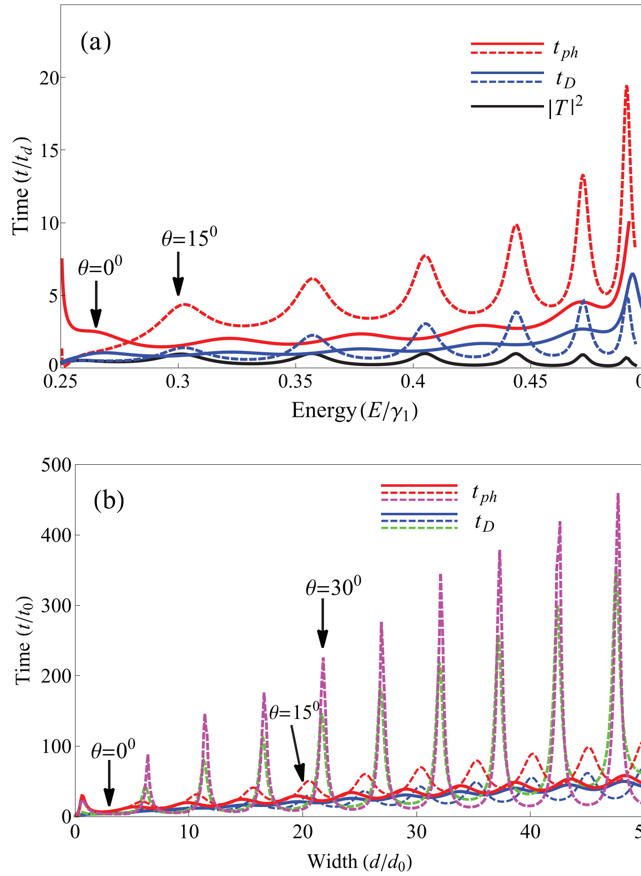

FIG. 3. (Color online) Tunneling times when ($u = 0.25\gamma_1$, $v_3 = 0$) ($\gamma_1 = 0.4$ eV). (a) Phase ($t_{\rm ph}$) and dwell (t_D) times vs energy for $d = 50d_0$. The solid black line displays the resonant transmission probability $|T|^2$ for the incident angle $\theta = 15^\circ$: note the local maxima of $t_{\rm ph}$ and t_D coincide with the resonance maxima. (b) Phase and dwell times vs barrier width for $E = 0.3\gamma_1$. The solid red and blue lines are for normal incidence: note they oscillate and increase with d, showing disappearance of the Hartman effect. Here, $V_0 = 0.75\gamma_1$, $d_0 = \hbar v_F/\gamma_1 = 1.48$ nm, $t_0 = d_0/v_F = 1.65$ fs, and $t_d = d/v_F = 50t_0 = 82.5$ fs.

effect does not exist when there are traveling waves with real or complex wave vectors inside the barrier.

2. *In the presence of band gap*

We now consider the effect of the band gap produced by an external gate field. In the presence of the band gap and without considering the TW term (i.e., when $u \neq 0$ and $v_3 = 0$), the x component of the pseudospinor eigenfunctions are again oscillating waves or evanescent waves and can be expressed as

$$\varphi_{\tau s}(x) = \begin{pmatrix} \chi_{s\tau}(k) \\ -s\chi_{-s\tau}(k)\,e^{\pm 2i\theta} \end{pmatrix} e^{\pm ik_x x} \quad \text{or}$$

$$\begin{pmatrix} \chi_{s\tau}(\kappa) \\ s\chi_{-s\tau}(\kappa)e^{\pm 2\theta_\kappa} \end{pmatrix} e^{\pm\kappa_x x}, \tag{17}$$

$$\chi_{\pm s\tau}(k) = \sqrt{\frac{E \pm \tau s\lambda_u}{2E}}, \quad E = \sqrt{\epsilon_k^2 + \lambda_u^2}.$$

Here, θ_κ is a positive value, satisfying $\kappa \sinh\theta_\kappa = -k\sin\theta$, and $\chi_{\tau s}(\kappa)$ for the evanescent waves can be obtained by the replacement of $k^2 = \kappa^2 + 2u^2/d_0^2(\gamma_1^2 + u^2)$ ($d_0 = \hbar v_F/\gamma_1 = 1.48$ nm): see Appendix B 1 b for explicit expressions of k and κ and the regional wave vectors. Using these pseudospinors, the transition probability (11) for the transmission across a junction is obtained as

$$W(k_f,k_i) = \frac{EE_2 - \left[\lambda_u\lambda_{u2} + \epsilon_k\epsilon_{k_2}\cos 2(\theta_2 - \theta)\right]}{2EE_2}, \quad (18)$$

where $E_2 = V_0 - E = \sqrt{\epsilon_{k_2}^2 + \lambda_{u2}^2}$ with $\lambda_{u2} = u - \hbar^2 k_2^2/2m_u$, $\theta_2 (= \pi - \beta_t \text{or} \pm\theta_{\kappa_2})$ is a scattering angle, and $\cos 2(\theta_2 - \theta) \to e^{\pm 2\theta_\kappa}\cos 2\theta$ for the imaginary wave vector as before. For the reflection, the negative sign should be changed to positive sign with $E_2 \to E$ and $\theta_f = \pi - \theta_r$ or θ_κ. From this, one can readily verify $W(k_f,k_i) \neq 0$ for the transmission and reflection [48]. Thus the incident wave can be scattered into any states (oscillating or evanescent waves) both in the reflection and transmission regions. This implies all amplitudes in Eq. (6) have nonzero values and hence the Klein effect disappears; the band gap destroys the chirality-induced orthogonal relation between the incident pseudospinor and the transmitted pseudospinors linked to the real wave vectors.

In Fig. 3(a), we present the phase and dwell times as a function of the incident energy. In this case, the incident flux is $\boldsymbol{j}_{\text{in}} = (1/E)(\epsilon_k v_k - \lambda_u v_u)\cos\theta\,\mathbf{e}_x$, where E is given in Eq. (17) and $v_k = \hbar k/m$, $v_u = \hbar k/m_u$; the dwell time will be longer for a lager incident angle. We should remark here that, although the eigenfunctions $\varphi_{\tau s}(x)$ are dependent on the valley index, the results in Fig. 3 are the same for both of the K and K' valleys because of the isotropic property. From the results, we find the tunneling times of the normal and an oblique incidences oscillate with increasing amplitude and local maxima corresponding to the resonant transmissions (see the solid black line). The resonance positions are

$$\begin{aligned} E_n &= V_0 - \sqrt{\frac{\left[(\gamma_1^2 + u^2)h_n^2 - u^2\right]^2 + \gamma_1^2 u^2}{\gamma_1^2 + u^2}}, \\ h_n &= \frac{n\pi d_0}{d\cos\beta_t}, \end{aligned} \quad (19)$$

where $d_0 = \hbar v_F/\gamma_1 = 1.48$ nm and n are positive integer such that $u < E_n < V_0 - u$. Again, this is a consequence of the Fabry-Pèrot-type interference inside the barrier. We also observe the amplitudes of oscillations grow as the incident angle becomes larger as expected from the smaller incident flux; from numerical simulations, we found that the maxima become peaks at larger angles, similar to the results in Fig. 2(a).

Figure 3(b) shows dependence on the barrier width of the tunneling times. As anticipated from the previous discussion they also oscillate with the barrier width, having peaks at larger angles: the interval is $\Delta d = \pi/(k_{2t}\cos\beta_t)$, where k_{2t} is given in Eq. (B3) with the replacement of $E \to V_0 - E$. We, however, emphasize that, in contrast to the case of no band gap, the Hartman effect disappears even for the normal incidence (see the solid lines indicated by $\theta = 0°$). Obviously, this is because traveling waves corresponding to the real wave vectors exist inside the barrier, which in turn produce finite particle velocities: in the present case the velocity is given by $v_{2tx} = (1/E_2)[\epsilon_{k_2} v_{k_2}\cos(\beta_{2t} - \theta) - \lambda_{u2} v_{u2}\cos\theta]$, where $v_{k_2} = \hbar k_2/m$, $v_{u_2} = \hbar k_2/m_u$, $E_2 = V_0 - E$, and β_{2t} is determined from the conservation relation (8).

In the present and previous results, we recognize that the phase time is longer than the dwell time. However, except for the case of normal incidence without band gap, a simple relationship between them is not available; direct application of the relation (16) yields complex interference time. This is because both of the oscillating and evanescent waves are allowed in the region I, whereas only oscillating waves are present in the ordinary barrier tunneling. For a detailed analysis, it would be necessary to use wave packet approach [49,50]. As a qualitative explanation, the extra delay in the phase time can be ascribed to a temporary stay of particles in front of the barrier due to the evanescent wave $e^{\kappa x}$ as well as the self-interference delay due to the oscillating waves $e^{ik_i x}$ and $e^{-ik_r x}$.

B. Tunneling times when the TW is included

When the TW is included the eigenspectrum is distorted to have anisotropic dispersion, as shown in Fig. 1(b). The major change here is that the wave vectors have valley dependence and their magnitudes change with the incident angle. From Eq. (3) and Appendix B 2, the wave vectors in the Klein-effect regime have two real values with opposite signs (k_τ or $-k_{\tau r}$) or two complex conjugate values ($k_{\tau c} = \tau k_c \pm i\kappa_c$). Thus the corresponding waves are all propagating waves, two of them with increasing or decreasing amplitude.

1. In the absence of band gap

In the absence of the band gap and when $v_3 \neq 0$, the eigenspectrum (2) becomes $E_\tau = E = \pm\lambda_{\tau k}$ ($E > 0$) and the pseudospinor eigenfunctions are

$$\begin{aligned} \varphi_{\tau s}(x) &= \frac{1}{\sqrt{2}}\begin{pmatrix} 1 \\ -se^{i\delta_\tau}\end{pmatrix} e^{ik_{\tau x}x}, \quad \frac{1}{\sqrt{2}}\begin{pmatrix} 1 \\ -se^{i\delta_{\tau r}}\end{pmatrix} e^{-ik_{\tau rx}x}, \\ \text{or} &= \frac{1}{\sqrt{2}}\begin{pmatrix} 1 \\ -se^{i\eta_\tau}\end{pmatrix} e^{ik_{\tau cx}x}, \quad (k_{\tau cx} = \tau k_{cx} \pm i\kappa_{cx}), \end{aligned} \quad (20)$$

where $k_{\tau x}, k_{\tau rx}, k_{cx}, \kappa_{cx} > 0$: see (B7) for the choice of regional wave vectors. The real phases δ_τ and $\delta_{\tau r}$ are given in Eqs. (3) and (7), and the complex phase is $\eta_\tau = \delta_\tau(k_{\tau c},\theta_c)$, where $k_{\tau c}$ and θ_c are determined from the conservation relation $k_{\tau c}\sin\theta_c = k\sin\theta$. The transition probability from these pseudospinors is

$$W(k_f,k_i) = \tfrac{1}{2}[1 + s_i s_f\cos(\delta_{\tau f} - \delta_{\tau i})]. \quad (21)$$

An interesting feature appears in the normal incidence. In this case, since $\theta = 0$, from the conservation relations (8) and (9) we have $\theta_r = \beta_t = \beta_r = \theta_c = 0$. This leads to $\delta_{\tau f} - \delta_{\tau i} = 2\pi$ for the reflection and transmission. The chiral transition probabilities are then evaluated to be $W(k_{2\tau tx},k_{\tau x}) = W(-k_{2\tau rx},k_{\tau x}) = W(\tau k_{2cx} \pm i\kappa_{2cx},k_{\tau x}) = 0$ for the transmission and $W(-k_{\tau rx},k_{\tau x}) = W(\tau k_{cx} - i\kappa_{cx},k_{\tau x}) = 1$ in the reflection region: see Eq. (B8) for explicit expressions of the wave vectors. Thus scattering across the junction ($n \to p$) is completely forbidden and the incident wave is totally reflected, leading to the Klein effect of perfect reflection.

From the matching conditions, we find all amplitudes in Eq. (6) are zero except A_τ and R_τ; omitting the subscript x since $k_x = k$ for normal incidence,

$$\begin{aligned} R_\tau &= \frac{k_{\tau\text{in}} + i\kappa_c}{k_{\tau\text{in}} - i\kappa_c} = e^{i\Delta\phi_{\tau r}}, \\ A_\tau &= -\frac{2k_{\tau\text{in}}}{k_{\tau\text{in}} - i\kappa_c}, \\ \Delta\phi_{\tau r} &= \arctan\left(\frac{2k_{\tau\text{in}}\kappa_c}{k_{\tau\text{in}}^2 - \kappa_c^2}\right), \\ k_{\tau\text{in}} &= k_\tau - \tau k_c = k_{\tau r} + \tau k_c, \end{aligned} \tag{22}$$

where the modulus $|R_\tau| = 1$, $\Delta\phi_{\tau r}$ is the phase delay of the perfection reflection, $k_\tau = (1/\hbar)\sqrt{2mE + m^2 v_3^2} + \tau k_c$, $k_{\tau r} = k_\tau - 2\tau k_c$, $k_c = m v_3/\hbar$ and $\kappa_c = (1/\hbar)\sqrt{2mE - m^2 v_3^2}$ from Eq. (B8) with the replacement of $d_0 = \hbar v_F/\gamma_1 = \hbar/2mv_F$. Using the given relations, one can easily show $R_{K'} = R_K$, $A_{K'} = A_K$ and $\Delta\phi_{K'r} = \Delta\phi_{Kr}$. To see the perfect reflection, we use the definition of $\boldsymbol{j}$ in Eq. (10) to evaluate the incident and reflected fluxes (at $x \to -\infty$). First, we note $E_\tau = \lambda_{\tau k} = \epsilon_k - \tau\hbar k v_3$ when $u = 0$. For normal incidence, $\theta = 0$ and $\delta_\tau = 0$, from which the incident flux is $\boldsymbol{j}_{\tau\,\text{in}} = (\hbar k_\tau/m - \tau v_3)\,\mathbf{e}_x$. For the reflected flux, $\theta_r = 0$ and $\delta_{\tau r} = 0$ from (3) and (7), so that $\boldsymbol{j}_{\tau\,\text{re}} = \langle\psi_{\tau\,\text{re}}|\hat{\boldsymbol{v}}|\psi_{\tau\,\text{re}}\rangle = -|R|^2(\hbar k_{\tau r}/m + \tau v_3)\mathbf{e}_x = -|R|^2(\hbar k_\tau/m - \tau v_3)\mathbf{e}_x$, where the relation $k_{\tau r} = k_\tau - 2\tau m v_3/\hbar$ has been used. The reflection probability is thus $\mathcal{P}_R = |\boldsymbol{j}_{\tau\,\text{re}}/\boldsymbol{j}_{\tau\,\text{in}}| = |R|^2 = 1$. In fact, for a BLG n-p junction (i.e., the potential step with height V_0), one can have the same results as (22). It should be noted here that, including the TW term, no particles can penetrate the barrier, even if it has finite width and height; when the TW is excluded (considered in Sec. III A 1) the Klein effect is a selective transmission, so that, although the probability is exponentially small, the quasiparticles are allowed to penetrate through the barrier. The present Klein effect of perfect reflection is another consequence of the chiral property of quasiparticles in BLG and should be considered as the effect of the trigonal warping.

Since there is no transmission at all, we cannot think of the dwell time which requires finite probability of finding particles inside the barrier region. By the same reason, there is no phase time associated with transmission. Consequently, it is not necessary to concern the Hartman effect here. However, from the expression of R_τ in Eq. (22), we can anticipate a phase time for the reflection as it contains the phase delay $\Delta\phi_{\tau r}$. Using the definition in Eq. (12), the phase time is found as

$$t_{\tau\text{ph}} = \left(\frac{k_c^2}{k_{\tau\text{in}}^2 - k_c^2}\right)\frac{2m}{\hbar k_{\tau\text{in}}\kappa_c} = \left(\frac{k_c^2}{k_\tau k_{\tau r}}\right)\frac{2m}{\hbar k_{\text{in}}\kappa_c}. \tag{23}$$

We remark here that, from the equality $\Delta\phi_{K'r} = \Delta\phi_{Kr}$, the above phase time is the same for the K and K' valleys, that is, $t_{K\text{ph}} = t_{K'\text{ph}}$.

The perfect reflection is reminiscent of the ordinary reflection of particles from a potential step in the Schrödinger equation [51]; in this case, the reflection amplitude is $R_{\text{od}} = (k_0 - i\rho)/(k_0 + i\rho)$ with the phase delay of $\Delta\phi_{\text{od}} = \arctan[2k_0\rho/(\rho^2 - k_0^2)]$ and the corresponding phase time is given by $t_{\text{od}} = 2m/\hbar k_0\rho$, where $k_0 = (1/\hbar)\sqrt{2m\epsilon_k}$ and $\rho = (1/\hbar)\sqrt{2m(V_0 - \epsilon_k)}$ [52]. In Fig. 4, for comparison, we plot t_{od} (the dashed line) as well as t_{ph} (the solid line) within the Klein-effect regime. As can be seen from the graphs, t_{ph} of the BLG barrier monotonically decreases, whereas t_{od} of the ordinary potential step increases as the energy approaches lower and higher limits. Of course, this difference stems from the different sources of the phase delays. In the ordinary potential step, the phase delay $\Delta\phi_{\text{od}}$ is originated from the nonzero probability of finding the particles inside the step. In the BLG barrier (or step), however, no particles are allowed inside the barrier (or step) region. To interpret the phase time in the BLG, we first observe a formal similarity between R_τ and R_{od}: comparing them one can regard $k_{\tau\text{in}} = k_\tau - \tau k_c$ ($k_{\tau\,\text{re}} = k_{\tau r} + k_{\tau c}$) and $-\kappa_c$ as an effective incident (reflected) wave vector and an evanescent wave vector corresponding to k_0 and ρ in the ordinary reflection, respectively. More explicitly, the effective incident (reflected) wave vector is related to the incident (reflected) velocity, that is, $\boldsymbol{k}_{\tau\text{in}} = m\boldsymbol{v}_{\tau\,\text{in}}/\hbar(\boldsymbol{k}_{\tau\,\text{re}} = m\boldsymbol{v}_{\tau\,\text{re}}/\hbar)$, where $\boldsymbol{v}_{\tau\,\text{in}} \equiv \boldsymbol{j}_{\tau\,\text{in}} = (\hbar k_\tau/m - \tau v_3)\mathbf{e}_x$ ($\boldsymbol{v}_{\tau\,\text{re}} \equiv \boldsymbol{j}_{\tau\,\text{re}} = -\boldsymbol{j}_{\tau\,\text{in}}$) from Eq. (10); the incident (reflected) particles can be described by the effective waves with wave vector $k_{\tau\,\text{in}}$ ($-k_{\tau\,\text{re}} = -k_{\tau\,\text{in}}$). For the correspondence of κ_c to ρ, one may replace ρ by $-\kappa_c$: the negative sign indicates that an effective evanescent wave exists in front of the barrier (i.e., $x < 0$). From this analogy κ_c seems to play the similar role as the evanescent wave vector ρ inside the ordinary potential step. In addition, there can also exist a delay due to the self-interference between the effective incident wave $e^{ik_{\tau\text{in}}x}$ and the reflected wave $e^{-ik_{\tau\,\text{re}}x}(=e^{-ik_{\tau\text{in}}x})$ in front of the barrier. Thus we may interpret the phase time $t_{\tau\text{ph}}$ as if the quasiparticles stay for a while in front of the barrier (within an effective length $\sim k_c^2/k_\tau k_{\tau r}\kappa_c$) before they are reflected back.

For an oblique incidence, the transition probability (21) has nonzero value for all scattering states, so that the transition from the incident wave to any scattering states, both in the reflection and transmission regions, are possible. Moreover,

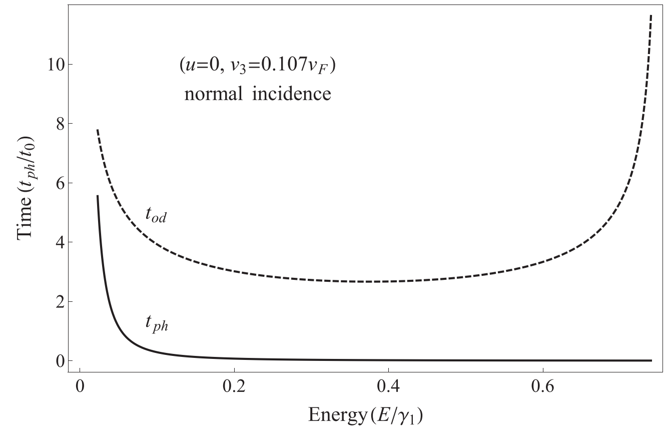

FIG. 4. Phase times vs energy for normal incidence when ($u = 0$, $v_3 = 0.107v_F$): t_{ph} is the phase time of the perfect reflection (solid line) from the BLG barrier with height $V_0 = 0.75\gamma_1$ ($\gamma_1 = 0.4$ eV) and t_{od} is the phase time of the reflection (dashed line) from the ordinary potential step (with height V_0) in Schrödinger equation. Note there is no dwell time in this case. The time scale is $t_0 = \hbar/\gamma_1 = 1.65$ fs.

since the scattering states inside the barrier are all traveling waves, resonant transmissions and finite particle velocities will be induced. The tunneling times are then expected to have similar behaviors as in the previous section: there are periodic peaks and it takes longer time to traverse the barrier as its width increases. An important difference from the previous cases is the tunneling times of quasiparticles at the K and K' valleys will behave differently. Since the types of wave vectors are the same both in the absence and presence of the band gap we will discuss this valley dependence of tunneling times together in the following section.

2. *In the presence of band gap*

Finally, we consider when both the TW and the band gap exist. In this case, the pseudospinor eigenfunctions can be expressed as

$$\begin{aligned} \varphi_{\tau s}(x) &= \begin{pmatrix} \chi_{s\tau}(k_\tau) \\ -s\chi_{-s\tau}(k_\tau)e^{i\delta_\tau} \end{pmatrix} e^{ik_{\tau x}x}, \\ &\quad \begin{pmatrix} \chi_{s\tau}(k_{\tau r}) \\ -s\chi_{-s\tau}(k_{\tau r})e^{i\delta_{\tau r}} \end{pmatrix} e^{-ik_{\tau rx}x}, \\ \text{or } &= \begin{pmatrix} \chi_{s\tau}(k_{\tau c}) \\ -s\chi_{-s\tau}(k_{\tau c})e^{i\eta_\tau} \end{pmatrix} e^{ik_{\tau cx}x}, \qquad (24) \\ &\quad (k_{\tau cx} = \tau k_{cx} \pm i\kappa_{cx}), \\ \chi_{\pm s\tau}(k) &= \sqrt{\frac{E_\tau \pm \tau s\lambda_u}{2E_\tau}}, \quad E_\tau(k) = \sqrt{\lambda_{\tau k}^2 + \lambda_u^2}, \end{aligned}$$

where $\lambda_{\tau k}$ and λ_u are given in Eq. (2), and $k_{\tau x}, k_{\tau rx}, k_{cx}, \kappa_{cx} > 0$: see (B7) for the choice of regional wave vectors. The real phases δ_τ and $\delta_{\tau r}$ are given in Eqs. (3) and (7) and the complex phase can be obtained from $\eta_\tau = \delta_\tau(k_{\tau c}, \theta_c)$. The corresponding transition probability is the same as (11).

We first examine the normal incidence, for which the phase difference in Eq. (11) is $\delta_{\tau f} - \delta_{\tau i} = 2\pi$ for the transmission. In contrast to the result in Fig. 4 where transmission is forbidden, the transition probability $W(k_f, k_i)$ has nonzero values [48], so that scattering into all states are possible in the transmission and reflection regions. As in the second case in Sec. III A, the presence of band gap destroys the orthogonal property between the incident and scattered pseudospinors to allow oscillating waves as transmission channels inside the barrier and hence the Klein effect of perfect reflection disappears.

Inside the barrier, since the wave vectors are $k_{2\tau tx}, -k_{2\tau rx}$, and $k_{2\tau cx} = \tau k_{2cx} \pm i\kappa_{2cx}$, there are two pure oscillating waves propagating in opposite directions or two forward (backward) propagating waves for the K valley (K' valley) each with decaying or growing amplitude, respectively. As before, these waves will undergo the Fabry-Pèrot-type interference to produce resonant transmissions and hence peaks of the tunneling times at the resonant maxima will occur. We demonstrate these features in Fig. 5 by plotting the phase and dwell times as functions of the incident energy and barrier width. Here, by setting $\theta = \delta_\tau = 0$ in the definition (10), the incident flux is given by $\boldsymbol{j}_{\tau\text{in}} = (1/E_\tau)[\lambda_{\tau k}(v_k - \tau v_3) - \lambda_u v_u]\mathbf{e}_x$, where $\lambda_{\tau k} = \epsilon_k - \tau\hbar k v_3$, $v_k = \hbar k/m$, and $v_u = \hbar k/m_u$. Comparing to the results for the normal incidence in Fig. 3 (the solid lines), we observe the tunneling times have sharp peaks rather than oscillations with small amplitude. In fact, the behaviors of the tunneling times are similar to the results for the oblique incidences in Fig. 3, exhibiting no Hartman effect. This shows the inclusion of the TW also produces significant changes in the tunneling times in the presence of the band gap as well as in the case without the band gap. In passing to the next discussion we emphasize here that the results in Fig. 5 are the same for both the K and K' valleys, showing no valley dependence for the normal incidence.

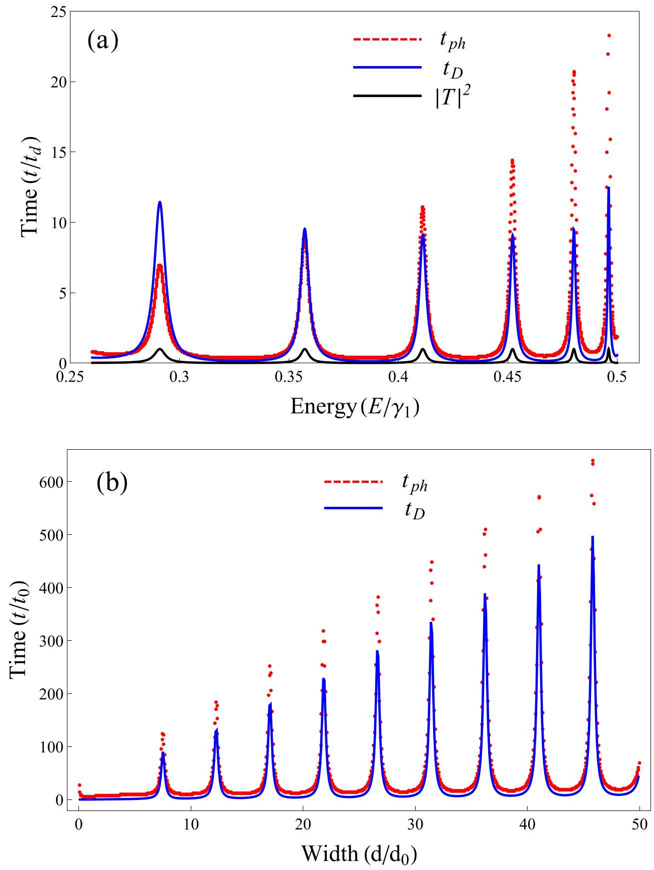

FIG. 5. (Color online) Tunneling times for normal incidence when ($u = 0.25\gamma_1$, $v_3 = 0.107v_F$). Phase ($t_{\rm ph}$) and dwell (t_D) times vs (a) energy for $d = 50d_0$ and (b) barrier width when $E = 0.3\gamma_1$. The solid black line in (a) displays the resonant transmission probability $|T|^2$. Here, $V_0 = 0.75\gamma_1$, $d_0 = \hbar v_F/\gamma_1 = 1.48$ nm, $t_0 = \hbar/\gamma_1 = 1.65$ fs, and $t_d = d/v_F = 50t_0 = 82.5$ fs.

For an oblique incidence, the transition probability (11) always has nonzero values for energies within the Klein-effect regime. Thus all scattering states inside the barrier are allowed as transmission channels and hence similar results as previous cases are expected: peaks of the tunneling times at resonant transmission maxima and longer times as the barrier width increases. However, the tunneling times now have valley dependence because of the anisotropic property of the energy dispersion. In Fig. 6, we plot dwell time as functions of the incident energy and the barrier width: for illustrative purpose we only display the dwell time because the phase time has the same behavior (with larger values) as can be seen from the previous results. From the figure, it can be clearly seen that the K- and K'-valley dwell times behave differently; at low energies the peaks of the K' valley is much smaller than those of the

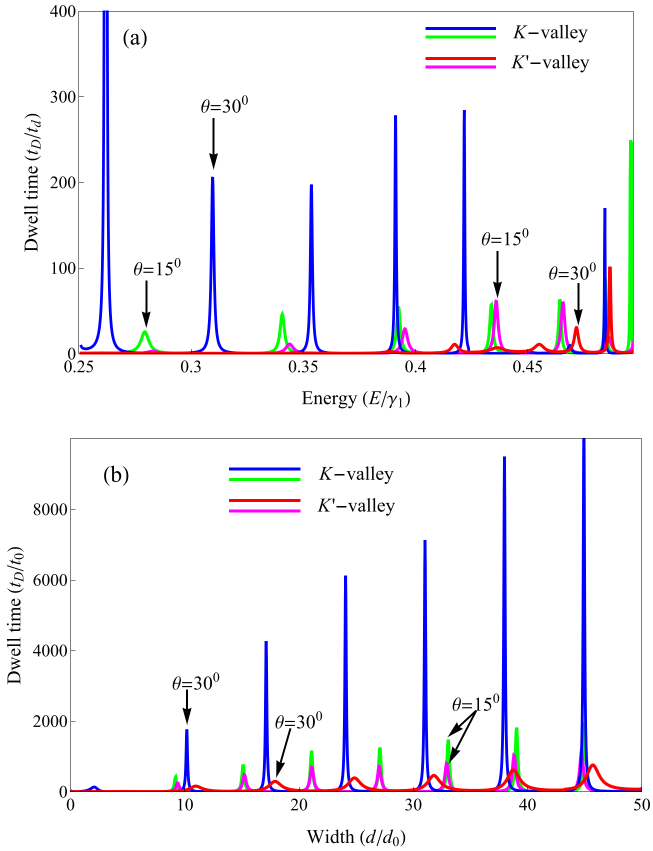

FIG. 6. (Color online) Dwell (t_D) time for oblique incidences ($\theta = 15^\circ$ and 30°) when $u = 0.25\gamma_1$ and $v_3 = 0.107v_F$ ($\gamma_1 = 0.4$ eV). (a) t_D vs energy for $d = 50d_0$ and (b) t_D vs barrier width when $E = 0.4\gamma_1$. The magnitude of t_D of the K' valley for $\theta = 30^\circ$ (the red line) in (b) has been 5 times scaled up for comparison. Note the dwell times of the K and K' valleys exhibit different behaviors because of the symmetry-breaking TW term. Here, $V_0 = 0.75\gamma_1$, $d_0 = \hbar v_F/\gamma_1 = 1.48$ nm, $t_0 = d_0/v_F = 1.65$ fs, and $t_d = d/v_F = 50t_0 = 82.5$ fs.

K valley and the positions of the peaks are off each other. By comparing these with the results for normal incidence in Fig. 5, it can be seen that the difference of tunneling times between the two valleys become more apparent as the incident angle increases. The main reason for the difference in the peak values can be understood from the different values of the incidence fluxes between the two valleys; from Fig. 1(b), one can see the x component of $\boldsymbol{j}_{K'\text{in}}$ is larger than $\boldsymbol{j}_{K\text{in}}$ for a given incident angle θ, so that the K'-valley dwell time is shorter. This is another consequence of the inclusion of the TW, which destroys the valley symmetry. For the split of the peak positions, we note from the resonance condition (19) that the position of the resonance is related to $d\cos\beta_t$, which has different values for the two valleys because $\beta_{Kt} \neq \beta_{K't}$ from Fig. 1(b).

The valley-dependent transmission makes the quasiparticles of the K and K' valleys emerge at different angles at the transmission region, that is, a valley-polarized scattering occurs in the presence of the TW. The scattering angles are determined by the directions of the fluxes at region III, which are the same as the incident fluxes. As we can see from Fig. 1(b), for the range of incident angles determined by the condition $J_{\tau x} > 0$, the K-valley particles will be scattered at larger angles than the K'-valley particles for the present choice of crystal orientation. Taking into account this and from the results in Fig. 6(a), we can expect the quasiparticles belonging to each valley will emerge at different time and angle. As numerical examples we take the second peaks (i.e., the second resonant positions) of the K valley in Fig. 6(a); when $\theta = 15^\circ$, the position is $E = 0.34\gamma_1$ and the dwell times and scattering angles for each valley are ($t_{DK} \approx 46.3t_d$, $t_{DK'} \approx 3.3t_d$) and ($\theta_{j_K} \approx 31^\circ$, $\theta_{j_{K'}} \approx 3^\circ$); when $\theta = 30^\circ$, the position is $E = 0.31\gamma_1$ and the dwell times and scattering angles are ($t_{DK} \approx 206t_d$, $t_{DK'} \approx 0.024t_d$) and ($\theta_{j_K} \approx 52^\circ$, $\theta_{j_{K'}} \approx 8^\circ$), where $t_d = 50t_0 = 82.5$ fs. Thus, for the crystal orientation in Fig. 1(b), the K-valley particles are transmitted at larger angles than those of the K' valley. The time difference $t_{DK} - t_{DK'}$, however, can be either positive or negative depending on the incident energy and angle, so that particles from the K valley are transmitted earlier or later than those of the K' valley. The valley-dependent transmission can also be seen in Fig. 6(b) where the time difference is very large at the barrier widths of resonant transmissions of the K-valley particles: $t_{DK} - t_{DK'} \approx \mathcal{O}(10^3 t_0)$. As an application of this valley-dependent transmission, one can collect electrons scattered at different angles to produce valley-polarized electrons in BLG [53,54]. Because of the difference in their dwell times, these valley-polarized electrons will come out of the barrier at different times.

IV. CONCLUDING REMARKS

We have demonstrated that the chiral tunneling of quasiparticles in a BLG n-p-n junction can be affected by the trigonal warping and the band gap induced by an external gate field. Their effects on the chiral tunneling can be seen clearly in the behaviors of the tunneling times, that is, the phase and dwell times. In the absence of the band gap, for the normal incidence of particles, the chiral property brings about the Klein effects of exponentially small transmission probability when the TW is excluded and of perfect reflection when the TW is included. The former produces the same behaviors of tunneling times as the conventional barrier tunneling, but the latter yields a novel phase time originated from the phase delay in the perfect reflection. The perfect reflection from a barrier is another manifestation of the Klein effect in BLG due to the chirality of quasiparticles, and it is associated with the trigonal warping and should be discriminated from the Klein reflection in a potential step (i.e., n-p junction) [6]. An oblique incidence of particles and/or opening a band gap destroy the chirality-induced orthogonal property between the incident and scattered pseudospinors that is responsible for the Klein effects, allowing oscillating waves inside the barrier. These oscillating waves then undergo the Fabry-Pèrot-type interference to produce resonant transmissions. As a result of this, the tunneling times have peaks at the incident energies and barrier widths corresponding to the resonant transmissions.

The effect of the TW for an oblique incidence can also appear as a valley-polarized transmission. The K-valley quasiparticles are scattered at larger angles than those of the K' valley. Depending on the incident angle and energy the particles of one valley are transmitted faster than those of the other valley and the difference is significantly large at the resonant transmissions. This feature can be used for obtaining valley-polarized electrons in a bilayer graphene.

We have also found that, unlike the monolayer graphene, the Hartman effect can exist for the particles of normal incidence on the BLG junction when both the TW and band gap are absent, which is the same situation as the ordinary barrier tunneling where only pure evanescent waves are allowed inside the barrier. From this observation, it seems that the Hartman effect is closely related to the pure evanescent waves inside the barrier; when oscillating (i.e., propagating) waves are allowed inside the barrier the quasiparticles can actually traverse the barrier with finite velocities, so that the transmission time increases with the barrier width. In this sense, the present results may give an indirect support of the explanation of the Hartman effect, that is, the phase and dwell times of the ordinary barrier tunneling are not the traversal times but the storage times of number of particles under the barrier [43,47].

Finally, we comment on the energy range and experimental observation of the present results. As mentioned in Sec. I, most of the previous works on the transport of quasiparticles in the BLG are based on the quadratic dispersion of the low-energy eigenspectrum; the effect of the TW term is generally assumed to be limited in the energy range of $|E| < 0.25\gamma_1 \approx 0.1$ eV around which the linear term $\hbar k v_3$ in Eq. (2) starts to play more importantly. There is, however, no clear cut where to discard the TW term [31]. As we have shown here, the inclusion of the TW term gives qualitatively different chiral tunnelings in the BLG barrier, and the difference can be appreciated more clearly in view of the tunneling times. As for the experimental observation, the time-resolved optical spectroscopy techniques, which has been proposed for the measurement of the phase time in MLG [55], may be applied to measure the phase time in the BLG junction. According to this method, a two-color optical pump can be used to generate and control the quasiparticles [56–58], then using the two-color optical coherence absorption spectra the transmission current through the BLG junction can be observed in real time [59].

ACKNOWLEDGMENT

The present work is supported by the research fund of Dankook University (Grant No. 2013-113558).

APPENDIX A: VELOCITY OPERATOR

By performing the commutator, the explicit expression of the velocity operator $\hat{\boldsymbol{v}}$ is obtained as

$$\hat{\boldsymbol{v}} = \begin{pmatrix} -\tau(\hat{v}_{ux}\mathbf{e}_x + \hat{v}_{uy}\mathbf{e}_y) & -\hat{v}_{\tau x}^\dagger\mathbf{e}_x + i\hat{v}_{\tau y}^\dagger\mathbf{e}_y \\ -\hat{v}_{\tau x}\mathbf{e}_x - i\hat{v}_{\tau y}\mathbf{e}_y & \tau\left(\hat{v}_{ux}\mathbf{e}_x + \hat{v}_{uy}\mathbf{e}_y\right) \end{pmatrix},$$
$$\hat{v}_{\tau x} = \frac{\hat{\pi}}{m} - \tau v_3, \quad \hat{v}_{\tau y} = \frac{\hat{\pi}}{m} + \tau v_3, \quad \hat{v}_{ux,y} = \frac{\hat{p}_{x,y}}{m_u}, \tag{A1}$$

where $\hat{\pi} = \hat{p}_x + i\hat{p}_y$ ($\hat{p}_{x,y} = -i\hbar\partial_{x,y}$).

APPENDIX B: WAVE VECTORS

The chirality-dependent scattering crucially depends on the nature of wave vectors. Here, we classify the possible wave vectors in BLG. From the dispersion relation (2), for a given energy E, the explicit expressions of wave vectors can be found from the roots of the following quartic equation:

$$(1+\alpha^2)d_0^4k^4 - 2\tau r d_0^3k^3\cos 3\theta + (r^2 - 2\alpha^2)d_0^2k^2 + \alpha^2 - \epsilon^2 = 0, \tag{B1}$$
$$d_0 = \hbar v_F/\gamma_1, \quad r = v_3/v_F, \quad \alpha = u/\gamma_1, \quad \epsilon = E/\gamma_1,$$

where d_0 has dimension of length given by $d_0 = 1.48$ nm and, for notational convenience, we have introduced dimensionless parameters $r = 0.107$ for the effective velocity v_3, α for band gap, and ϵ for energy. Since we are interested in the Klein-effect regime, it is assumed $\alpha < \epsilon < v_0 - \alpha$ ($v_0 = V_0/\gamma_1$).

1. When the TW is excluded: $v_3 = 0$ ($r = 0$)

In this case, the eigenspectum is isotropic for $\boldsymbol{k}$; the wave vectors have the same magnitudes for all directions and no valley dependence.

a. In the absence of band gap: ($\alpha = 0, r = 0$)

In this case, the quartic equation becomes $d_0^4k^4 = \epsilon^2$ and hence there are two real roots $\pm\sqrt{\epsilon}/d_0 = \pm k$ or two imaginary roots $\pm i\sqrt{\epsilon}/d_0 = \pm i\kappa$. From Eq. (6), we choose the wave vectors at each region as follows:

$$\begin{aligned} k_{ix} &= k_{rx} = k_x, \quad k_{2rx} = k_{2tx} = k_{2x}, \\ q_{1x} &= -q_{3x} = -i\kappa_x, \quad \rho_{2x\pm} = \pm i\kappa_{2x}, \end{aligned} \tag{B2}$$

where $k_2 = \sqrt{\epsilon_2}/d_0 = \kappa_2$ with $\epsilon_2 = v_0 - \epsilon$ [see Eq. (5)] and the x components of the wave vectors at each region can be obtained from the conservation relations (8) and (9): the same procedure can also be applied in the following cases.

b. In the presence of band gap: ($\alpha \neq 0, r = 0$)

In this case, the quartic equation becomes $(1+\alpha^2)d_0^4k^4 - 2\alpha^2d_0^2k^2 + \alpha^2 - \epsilon^2 = 0$ and we have the same kinds of roots as the first case (i.e., two real or two imaginary roots), but they now depend on the gap parameter α. The explicit expressions of the wave vectors are

$$\begin{aligned} \pm k &= \frac{\pm 1}{d_0\sqrt{1+\alpha^2}}\sqrt{\alpha^2 + \sqrt{(1+\alpha^2)\epsilon^2 - \alpha^2}}, \\ \pm\kappa &= \frac{\pm 1}{d_0\sqrt{1+\alpha^2}}\sqrt{-\alpha^2 + \sqrt{(1+\alpha^2)\epsilon^2 - \alpha^2}}. \end{aligned} \tag{B3}$$

There is a simple relationship between k and κ:

$$k^2 = \kappa^2 + \frac{2\alpha^2}{d_0^2(1+\alpha^2)}. \tag{B4}$$

We choose the regional wave vectors as follows:

$$\begin{aligned} k_{ix} &= k_{rx} = k_x, \quad k_{2rx} = k_{2tx} = k_{2x}, \\ q_{1x} &= -q_{3x} = -i\kappa_x, \quad q_{2x\pm} = \pm i\kappa_{2x}, \end{aligned} \tag{B5}$$

where k_2 and κ_2 have the same expressions as (B3) with the replacement of $\epsilon \to \epsilon_2 = v_0 - \epsilon$.

2. When the TW is included: $v_3 = rv_F$ ($r \neq 0$)

In this case, the eigenspectrum is anisotropic for $\boldsymbol{k}$; the wave vectors have different magnitudes at different directions and valley dependence. The wave vectors are the roots of the quartic equation (B1). However, simple analytical expressions of the solutions are not available, although they can, in principle, be obtained. In the Klein-effect regime ($\alpha < \epsilon < v_0 - \alpha$), numerical evaluation reveals all roots are classified as following types:

$$k_\tau, \quad -k_{\tau r} \quad (k_\tau, k_{\tau r} > 0),$$
$$k_{\tau c} = \pm\tau k_c \pm i\kappa_c \quad (k_c, \kappa_c > 0), \tag{B6}$$

where τ is the valley index. In the second line, $+\tau$ and $-\tau$ exist when $0 \leqslant \theta < \pi/6$ and $\pi/6 < \theta < \pi/2$, respectively: in the text and following discussion, we shall only use the first case for a qualitative argument because the second case is just reverse of the roles of the K- and K'-valley wave vectors. The wave vectors at each region can be chosen as follows:

$$k_{ix} = k_{\tau x}, \quad k_{rx} = k_{\tau rx}, \quad k_{2ix} = k_{2\tau tx}, \quad k_{2rx} = k_{2\tau rx},$$
$$q_{1x} = (\tau k_c - i\kappa_c)_x, \quad q_{3x} = (\tau k_c + i\kappa_c)_x, \tag{B7}$$
$$q_{2x+} = (\tau k_{2c} + i\kappa_{2c})_x, \quad q_{2x-} = (\tau k_{2c} - i\kappa_{2c})_x,$$

where $k_{2\tau t}$, $k_{2\tau r}$, and $q_{2\pm}$ are the roots obtained from the replacement of $\epsilon \to \epsilon_2 = v_0 - \epsilon$ in the quartic equation (B1). Note the choice of the imaginary parts for q_{1x} and q_{3x}; although they produce left-traveling or right-traveling waves we have chosen wave vectors such that their amplitudes always decay as $x \to \pm\infty$. From this, we have peculiar wave in the region III such that $e^{-ik_{cx}x}e^{-\kappa_{cx}x}$; left-propagating waves in the transmission region.

a. Normal incidence in the absence of band gap: ($\alpha = 0, r \neq 0$)

In this special case, we can have analytical expressions for the wave vectors as follows:

$$k_\tau = \tau k_c + \sqrt{2k_c^2 + \kappa_c^2}, \quad -k_{\tau r} = -(k\tau - 2\tau k_c),$$
$$k_{\tau c} = \tau k_c \pm i\kappa_c, \quad k_c = \frac{r}{2d_0}, \quad \kappa_c = \frac{1}{2d_0}\sqrt{4\epsilon - r^2}. \tag{B8}$$

Inside the barrier region, the wave vectors are $k_{2\tau t}$, $k_{2\tau r}$, and $k_{2\tau c}$, which have the same expressions with the replacement of $\epsilon \to \epsilon_2$. Note that we have $+\tau$ in $k_{\tau c}$ because $\theta = 0$ for the normal incidence. There is an extra relation between k_τ and $k_{\tau r}$: $k_\tau = k_{\tau r} + 2\tau k_c$.

[1] C. W. J. Beenakker, Rev. Mod. Phys. **80**, 1337 (2008).
[2] A. H. Castro Neto, F. Guinea, N. M. R. Peres, K. S. Novoselov, and A. K. Geim, Rev. Mod. Phys. **81**, 109 (2009).
[3] S. D. Sarma, S. Adam, E. H. Hwang, and E. Rossi, Rev. Mod. Phys. **83**, 407 (2011).
[4] O. Klein, Z. Phys. **53**, 157 (1929).
[5] A. Calogeracos and N. Dombey, Contem. Phys. **40**, 313 (1999).
[6] M. I. Katsnelson, K. S. Novoselov, and A. K. Geim, Nat. Phys. **2**, 620 (2006); for extensive reviews on the Klein effects in graphene see Refs. [7–9].
[7] P. E. Allain and J. N. Fuchs, Eur. Phys. J. B **83**, 301 (2011).
[8] T. R. Robinson, Am. J. Phys. **80**, 141 (2012).
[9] T. Tudorovkkiy, K. J. A. Reijnders, and M. I. Katsnelson, Phys. Scr. **T146**, 014010 (2012).
[10] V. V. Cheianov and V. I. Fal'ko, Phys. Rev. B **74**, 041403(R) (2006).
[11] A. V. Shytov, M. S. Rudner, and L. S. Levitov, Phys. Rev. Lett. **101**, 156804 (2008).
[12] R. V. Gorvachev *et al.*, Nano. Lett. **8**, 1995 (2008).
[13] A. F. Young and P. Kim, Nat. Phys. **5**, 222 (2009).
[14] N. Stander, B. Huard, and D. Goldhaber-Gordon, Phys. Rev. Lett. **102**, 026807 (2009).
[15] R. Nandkishore and L. Levitov, Proc. Natl. Acad. Sci. USA **108**, 14021 (2011).
[16] S. Park and H.-S. Sim, Phys. Rev. Lett. **103**, 196802 (2009).
[17] S. Park and H.-S. Sim, Phys. Rev. B **84**, 235432 (2011).
[18] N. Agrawal (Garg), S. Grover, S. Ghosh, and M. Sharma, J. Phys.: Condens. Matter **24**, 175003 (2012).
[19] C. J. Poole, Solid State Commun. **150**, 632 (2010).
[20] C.-S. Park, Solid State Commun. **152**, 2018 (2012).
[21] T. Ohta, A. Bostwick, T. Seyller, K. Horn, and E. Rotenberg, Science **313**, 951 (2006).
[22] L. M. Zhang, Z. Q. Li, D. N. Basov, M. M. Fogler, Z. Hao, and M. C. Martin, Phys. Rev. B **78**, 235408 (2008).
[23] E. V. Castro, K. S. Novoselov, S. V. Morozov, N. M. R. Peres, J. M. B. Lopes dos Santos, J. Nilsson, F. Guinea, A. K. Geim, and A. H. Castro Neto, J. Phys.: Condens. Matter **22**, 175503 (2010).
[24] Y. Zhang *et al.*, Nature (London) **459**, 820 (2009).
[25] A. B. Kuzmenko, I. Crassee, D. van der Marel, P. Blake, and K. S. Novoselov, Phys. Rev. B **80**, 165406 (2009).
[26] K. F. Mak, C. H. Lui, J. Shan, and T. F. Heinz, Phys. Rev. Lett. **102**, 256405 (2009).
[27] G. M. Rutter, S. Jung, N. N. Klimov, D. B. Newell, N. B. Zhitenev, and J. A. Stroscio, Nat. Phys. **7**, 649 (2011).
[28] E. McCann and V. I. Fal'ko, Phys. Rev. Lett. **96**, 086805 (2006).
[29] E. McCann, Phys. Rev. B **74**, 161403(R) (2006).
[30] E. McCann, D. S. L. Abergel, and V. I. Fal'ko, Solid State Commun. **143**, 110 (2007).
[31] E. McCann and M. Koshino, Rep. Prog. Phys. **76**, 056503 (2013).
[32] We use $v_F = (\sqrt{3}/2)a\gamma_0/\hbar = 9 \times 10^5$ m/s, where $a = 2.46 \times 10^{-10}$ m is the lattice constant.
[33] A. S. Mayorov, D. C. Elias, M. Mucha-Kruczynski, R. V. Gorbachev, T. Tudorovskiy, A. Zhukov, S. V. Morozov, M. I. Katsnelson, V. I. Fal'ko, A. K. Geim, and K. S. Novoselov, Science **333**, 860 (2011).
[34] D. A. Gradinar, H. Schomerus, and V. I. Fal'ko, Phys. Rev. B **85**, 165429 (2012); A. J. Pearce, F. Cavaliere, and E. Mariani, J. Phys.: Condens. Matter **25**, 375301 (2013).
[35] In the eigenstate (3), the pseudospin polarization vector is $\boldsymbol{\sigma}_{\tau s} = \langle\psi_{\tau s}|\hat{\boldsymbol{\sigma}}|\psi_{\tau s}\rangle = (-s/E_\tau)[\lambda_{\tau k}(\cos\delta_\tau \mathbf{e}_x + \sin\delta_\tau \mathbf{e}_y) - \tau\lambda_u \mathbf{e}_z]$.
[36] The actual condition of overlap is $V_0 > 2E_{\min}$, where $E_{\min}$ is the minimum value of E and slightly lower than u. However, since we are interested in the energy range above the Lifshitz transition energy, the condition in this equation is sufficient for our purpose.

[37] T. Ando, T. Nakanishi, and R. Saito, J. Phys. Soc. Jpn. **67**, 2857 (1998).

[38] H. G. Winful, Phys. Rep. **436**, 1 (2006).

[39] *Time in Quantum Mechanics*, edited by J. G. Muga, R. Sala Mayato, and I. L. Egusquiza, 2nd ed. (Springer, Berlin, 2008), Vol. 1.

[40] T. E. Hartman, J. Appl. Phys. **33**, 3427 (1962).

[41] For this choice of θ_κ, $\kappa_x = \cosh\theta_\kappa$ and $\kappa_y = -i\kappa \sinh\theta_\kappa$, with $\kappa_x^2 + \kappa_y^2 = \kappa^2 = 2mE/\hbar$.

[42] M. Büttiker, Phys. Rev. B **27**, 6178 (1983).

[43] H. G. Winful, Phys. Rev. Lett. **91**, 260401 (2003).

[44] F. T. Smith, Phys. Rev. **118**, 349 (1960).

[45] Z. Wu, K. Chang, J. T. Liu, X. J. Li, and K. S. Chan, J. Appl. Phys. **105**, 043702 (2009).

[46] D. Dragoman and M. Dragoman, J. Appl. Phys. **107**, 054306 (2010).

[47] H. G. Winful, New J. Phys. **8**, 101 (2006).

[48] One exceptional case is when $E = \lambda_u V_0/(\lambda_u + \lambda_{u_2})$ for the normal incidence, which gives $W(k_{2r},k) = W(-k_{2t},k) = 0$. Writing the condition as $\lambda_u/E = \lambda_{u_2}/E_2$, it is the same as the condition found in Ref. [17], for which the Klein effect survives in the presence of the band gap.

[49] E. H. Hauge and J. P. Falck, and T. A. Fjeldly, Phys. Rev. B **36**, 4203 (1987).

[50] E. H. Hauge and J. A. Støvneng, Rev. Mod. Phys. **61**, 917 (1989).

[51] Note a half-infinite wall also produces perfect reflection. In this case, however, the reflected wave has the constant phase shift of π and hence no phase time exists.

[52] C. Cohen-Tannoudji, B. Diu, and F. Laloë, *Quantum Mechanics* (Wiley, New York, 1977), Chap. 1.

[53] V. V. Cheianov, V. Fal'ko, and B. L. Altshuler, Science **315**, 1252 (2007).

[54] J. L. Garcia-Pomar, A. Cortijo, and M. Nieto-Vesperinas, Phys. Rev. Lett. **100**, 236801 (2008).

[55] J. T. Liu, F. H. Su, H. Wang, and X. H. Deng, New J. Phys. **14**, 013012 (2012).

[56] E. J. Mele, P. Král, and D. Tománek, Phys. Rev. B **61**, 7669 (2000).

[57] R. Atanasov, A. Haché, J. L. P. Hughes, H. M. van Driel, and J. E. Sipe, Phys. Rev. Lett. **76**, 1703 (1996).

[58] H. Zhao, X. Pan, A. L. Smirl, R. D. R. Bhat, A. Najmaie, J. E. Sipe, and H. M. van Driel, Phys. Rev. B **72**, 201302(R) (2005).

[59] J. T. Liu, F. H. Su, X. H. Deng, and H. Wang, Opt. Express **20**, 11694 (2012).